



PHYSICO-CHEMICAL CHARACTERIZATION AND ANTIBACTERIAL, ANTIFUNGAL AND ANTIVIRAL ACTIVITY OF TWO NEW BENZIMIDAZOLYPHENOL DERIVATIVES AND THEIR COMPLEXES

Dildora PARDAEVA,^a Aydin TAVMAN,^{b,*} Demet GÜRBÜZ,^c Mayram HACIOĞLU,^d
Fatıma Nur YILMAZ,^d Adem CINARLI^c and A. Seher BIRTEKSÖZ TAN^d

^a Istanbul University-Cerrahpaşa, Institute of Graduate Education, Department of Chemistry, 34320, Avcılar, Istanbul, Türkiye

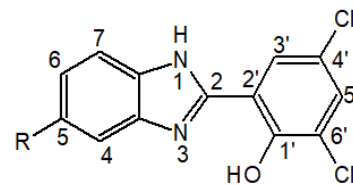
^b Istanbul University-Cerrahpaşa, Faculty of Engineering, Department of Chemistry,
Inorganic Chemistry Division, 34320, Avcılar, Istanbul, Türkiye

^c Istanbul University-Cerrahpaşa, Faculty of Engineering, Department of Chemistry,
Organic Chemistry Division, 34320, Avcılar, Istanbul, Türkiye

^d Istanbul University, Faculty of Pharmacy, Department of Pharmaceutical Microbiology, 34452, Beyazıt, Istanbul, Türkiye

Received April 26, 2025

Two new chelating benzimidazolylphenol type ligands, 2-(6-*tert*-butyl-1*H*-benzimidazol-2-yl)-4,6-dichlorophenol (**HL**¹) and 2,4-dichloro-6-(6-chloro-1*H*-benzimidazol-2-yl)phenol (**HL**²) were employed to create complexes (**1a** – **2e**) with Co(II), Ni(II), Cu(II), Zn(II) and Pd(II) ions. A variety of analytical and spectroscopic methods were utilized to verify the structures of the synthesized chelates, including elemental analysis, ¹H-NMR, UV-Vis spectroscopy, FT-IR, fluorescence spectroscopy, thermogravimetric analysis (TGA), magnetic moment and molar conductivity. The stoichiometry of the metal complexes was determined to be 1:2 M:L for Co(II) and Ni(II) complexes, while the Zn(II) and Pd(II) complexes exhibited a 1:1 M:L ratio. The antibacterial and antifungal activities of the compounds were tested against six bacteria and three fungi, and minimum inhibitory concentrations (MIC) values were obtained at the range of 39 – 1250 µg/mL. It was observed that **HL**² (chloro derivative) showed slightly higher activity than **HL**¹, while Ni(II), Zn(II) and Pd(II) complexes of both ligands were found to be more active against bacteria especially, compared to the ligands. Antiviral activity of the compounds was tested against Parainfluenza Type-2 virus. It was observed that **HL**¹ showed higher antiviral activity than **HL**² (antiviral property promoting effect of *tert*-butyl group) and the complexes showed higher antiviral activity than the ligands.



INTRODUCTION

Benzimidazole derivatives containing phenol groups, known as benzimidazolylphenols, are one of the current and widespread research topics, and these compounds have the potential for application in many biological and technical fields. One of the most important features of these compounds in

terms of coordination chemistry is that they form strong chelate complexes with a two-ring structure by coordinating to metals via phenolic oxygen and C=N nitrogen atoms. In addition, due to the strong fluorescence properties of these compounds, many studies have been published examining the photo-physical properties of them and their various metal complexes.¹⁻³

* Corresponding author: atavman@iuc.edu.tr (A. Tavman)

Numerous studies on the biological activities of many benzimidazolylphenol compounds and their complexes have been published. For instance, we reported that many benzimidazolyl-phenol derivatives and some of their metal complexes exhibited antimicrobial effect on some bacteria and fungi.⁴⁻¹² For example, 2-(5-nitro-1*H*-benzimidazol-2-yl)-bromophenol and its Zn(II), Fe(III) and Cu(II) complexes showed considerable antibacterial activity on *S. aureus* and *S. epidermidis*.^{13,14} It is observed that the Cl, Br and NO₂ groups increase the antimicrobial activity toward *S. aureus*, *E. faecalis* and *C. albicans* in some 5-methoxy-2-(5-substituted-1*H*-benzimidazol-2-yl)-phenols.¹⁵ The Au(III) complexes of 2-[4,6-(Cl/CH₃/CF₃)-benzimidazol-2-yl]-4-(OCH₃/Br)-phenols were found to have superior activity against all the bacteria, while the Pd(II) complexes showed higher antifungal activity than the ligands.¹⁶ In the study where the physicochemical and biological properties of 2-(5-Bromo-1*H*-benzimidazol-2-yl)-phenol and its Fe(III), Co(II), Ni(II), Cu(II), Zn(II) and Ru(III) complexes and many of its derivatives were investigated, it was determined that the derivatives carrying a second OH group in the phenol ring exhibited both antioxidant and antibacterial activities and it was suggested that there was a correlation between the antibacterial and antioxidant effects. It was also observed that the Ru(III) and Co(II) complexes showed moderate antibacterial activity whereas the ligand was inactive.¹²

The cytotoxic effects of Gd(III), Tb(III) and Dy(III) complexes of 2-(5-H/methyl-1*H*-benzimidazol-2-yl)-phenols (Bzp1 and Bzp2) were investigated and it was found that the complexes of Bzp2 ([Ln(Bzp2)₂(NO₃)₂]NO₃) showed moderate activity against HeLa cells.¹⁷ DNA-targeting properties of 2-(1*H*-benzimidazol-2-yl)-4-chlorophenol (BM1), 4-chloro-2-(6-methyl-1*H*-benzimidazol-2-yl)phenol (BM2) and 4-chloro-2-(6-nitro-1*H*-benzimidazol-2-yl)phenol (BM3) were investigated and found that the compound BM2 was found to be the effective DNA binding antimicrobial agent. Furthermore, the preliminary cytotoxic properties of BM1, BM2 and BM3 were evaluated by brine shrimps lethality assay to check their nontoxic nature towards healthy normal cells.¹⁸

As is known, Cu(II) and Zn(II) ions have important roles in the human body. Cobalt, which is a part of vitamin B12, is also an essential metal. Some Ni(II) and Pd(II) complexes have also been reported to have various biological activities.^{19,20}

In this study, it is aimed to synthesize two new benzimidazolylphenol ligands carrying *tert*-butyl

and chloro groups (Fig. 1) and to obtain their complexes with Co(II), Ni(II), Cu(II), Zn(II) and Pd(II) ions and compare their properties and activities on certain bacteria, fungi and also Parainfluenza type-2 virus.

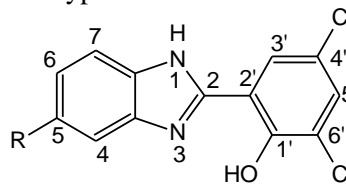


Fig. 1 – Chemical structures of the ligands in the study {R = C(CH₃), **HL**¹; R = Cl, **HL**²}.

RESULTS AND DISCUSSION

General Properties

The ligands have monobasic bidentate characteristic. Both ligands reacted with metal ions in similar M:L ratios to form complexes: This ratio is 1:2 in Co(II), Ni(II) and Cu(II) complexes (**1a** – **1c** and **2a** – **2c**); and 1:1 in Zn(II) and Pd(II) complexes (**1d**, **1e**, **2d** and **2e**).

The molar conductivity values of the complexes were measured to be below 50 Ω⁻¹cm²mol⁻¹ in DMF. According to Geary, these results show that all the complexes in this study have non-ionic characteristic.²¹

The magnetic moment value of the Co(II) complexes (**1a** and **2a**) was calculated from corresponding susceptibilities as 2.72 and 2.81 BM for **HL**¹ and **HL**², respectively. These values, which are only lower than the spin value for high spin and only higher than the spin value for low spin configurations, can be considered as a spin equilibrium between the two spin states, a high-spin state and a low-spin state, and it is possible to claim that the geometry is distorted tetrahedral.^{22,23} The magnetic moment values of the Ni(II) complexes (**1b** and **2b**) were found to be 1.21 and 1.31 BM for **HL**¹ and of **HL**², respectively. These anomalous values may be due to **1b** and **2b** having spin equilibrium between the two spin states such as in **1a** and **2a** mentioned above.²⁴⁻²⁶ As is known, the expected magnetic moment value for tetrahedral and high spin octahedral Ni(II) complexes is 2.8 BM; square planar complexes are diamagnetic. The magnetic moment value of the structure, which is a mixture of these two geometries or spin states, corresponds to approximately 1.4 BM. The magnetic moment values we found (1.31 and 1.21 BM) are very close to 1.4.

The magnetic moment values of Cu(II) complexes (**1c** and **2c**) were found to be 1.25 and

1.62 BM for **HL**¹ and **HL**² complexes, respectively. These data show that **1c** and **2c** have different structures. The low magnetic moment value of **1c** shows that there is a Cu-Cu interaction in this complex. Considering the elemental analysis values, it can be said that this complex has a 1:1 chlorine bridged dimeric structure having composition formula such as $[\text{Cu}_2(\text{L}^1)_2\text{Cl}_2]$. The magnetic moment value of **2c** shows that it is a typical monomeric Cu(II) complex. The magnetic moment value of **2c** (1.62 BM) is very close to the theoretical value of 1.71 BM for the d^9 electron configuration. Considering the elemental analysis data, it is possible to suggest that **2c** has a 1:2 M:L ratio having composition formula such as $([\text{Cu}(\text{L}^2)_2])$. It was observed that there was a difference in the complexation of **HL**¹ and **HL**² with CuCl_2 . The reason for this may be that the tertiary butyl group in **HL**¹ directs or forces its complex to a dimeric structure due to its steric effect. On the other hand, the different colors of the Cu(II) complexes is another finding that shows that their structures are different: color of **1c** is greenish brown, that of **2c** is brown.

Thermogravimetric Studies

The major features of the thermal analysis of the complexes are given in Experimental section.

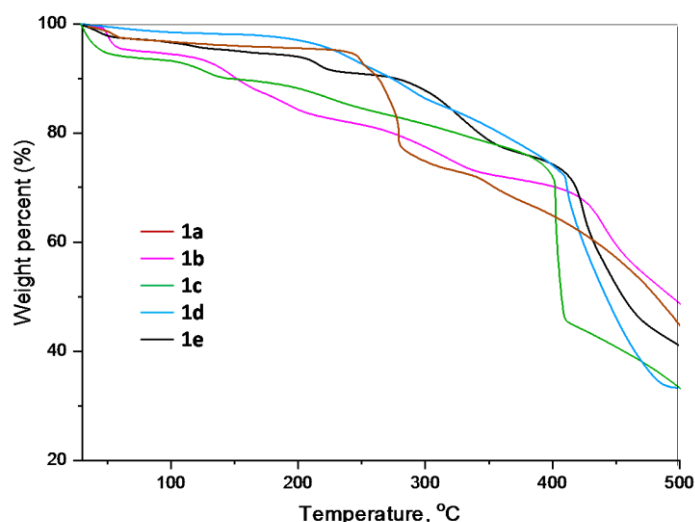


Fig. 2 – TGA curves of **HL**¹ complexes in the study.

In the third stage, the organic structure breaks down as various groups are separated from the ligands, and in the last stage, chemical changes are observed in the formation of the metal oxide.

From the differential thermal analysis (DTA) curves, the degradation temperatures of the

The thermal analysis curves of the **HL**¹ complexes are shown in Fig. 2. Samples of the complexes were heated from room temperature to 500 °C in air atmosphere. Thermal decomposition was observed to occur in four stages for most of the complexes. At the first stage, uncoordinated lattice water was lost through elimination from 40 to 100 °C. At the second stage, coordinated water molecules are removed above 100 °C. In the TGA curve of **1c**, a mass loss of ~7.5% was observed in the range of 60 – 90 °C corresponds to four moles of lattice water. A mass loss of around %5 below 100 °C in **1a**, **1b** and **2b** indicates that there is two moles of lattice water in each of these complexes. It is possible to suggest that one mole of water molecules is coordinated to Zn(II) ions considering the mass loss ~5% in the 150 – 200 °C range in the TGA curves of **1d** and **2d**. The absence of lattice or coordinated water molecules in **2a** and **2c** was also confirmed by TGA curves in agreement with other data such as FTIR and elemental analysis.

The mass loss between 3.5 – 4.0% seen below 100 °C in the TGA curves of both Pd(II) complexes (**1e** and **2e**) shows that one mole of water is in the lattice state in these complexes. This may lead us to the conclusion that there is a dimeric structure in both complexes.

complexes can be determined. In complexes with lattice or coordinated water molecules, removing of water molecules (dehydration) from the complex can be considered as the onset of decomposition temperature. Figure 3 shows the TGA and DTA curves of **1e**. The exothermic value observed at

420 °C as sharp peak indicates the decomposition temperature of it. Degradation degrees of the other

complexes compounds according to DTA are given in the experimental section.

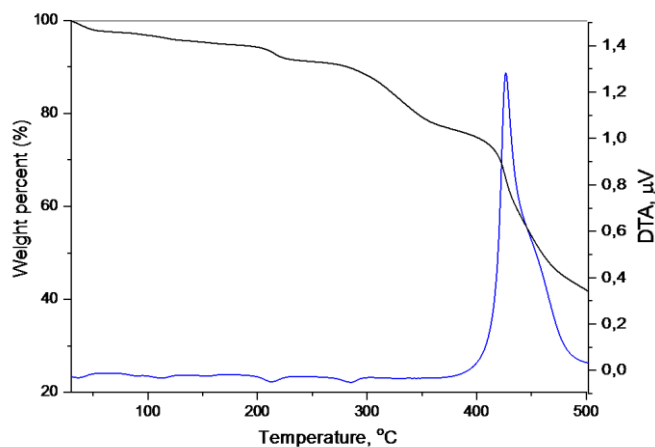


Fig. 3 – TGA and DTA curves of **1e**.

¹H-NMR Spectra

¹H-NMR spectral data and their assignments of the ligands and the diamagnetic Zn(II) and Pd(II) complexes are given in Experimental Section.

The broad singlets corresponding to two protons at 13.80 and 13.78 ppm for **HL**¹ and **HL**² ligands, respectively, belong to both NH and OH protons and are due to the formation of intramolecular hydrogen bonds between N and O atoms (Fig. 4).^{12,13} As a result of hydrogen bond formation, these protons show identical proton behavior. The phenolic proton is removed from Pd(II) and Zn(II) complexes (**1d**, **1e**, **2d**, **2e**) after

complex formation according to the ¹H-NMR spectra as expected. In the complexes, the NH proton appears as a broad singlet (integral value: 1H) in the range of 13.46 – 13.82 ppm. Comparative ¹H-NMR spectra of **HL**¹ and its Zn(II) and Pd(II) complexes are given in Fig. 5.

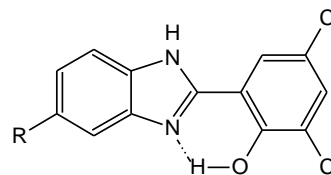


Fig. 4 – Intramolecular hydrogen bond formation in **HL**¹ and **HL**² ligands.

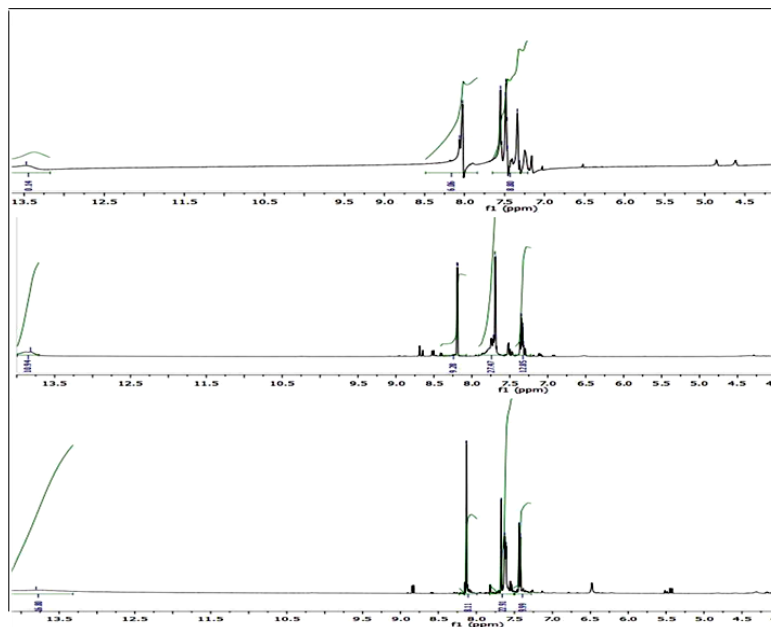


Fig. 5 – Comparative ¹H-NMR spectra of **HL**¹ and its Pd(II) and Zn(II) complexes.

No signals of coordinated water molecules were detected in the $^1\text{H-NMR}$ spectra of Zn(II) complexes (**1e** and **2e**) containing one mole of coordinated water according to the thermogravimetric data. The reason of this may be as follows: Since NMR spectra were taken in DMSO-d_6 , water molecules are dissociated or removed from the complex in the solvent. As a result, lattice water signals are observed around 3.5 ppm.

IR Spectra

The FTIR spectral data of the ligands and the complexes are presented in Experimental Section. The IR spectra of **HL**¹ and its complexes are given

comparatively in Fig. 6. The IR spectra of the ligands and the complexes shows medium intensity absorption bands at $1615\text{--}1668\text{ cm}^{-1}$ assigned to $\nu(\text{C}=\text{N})$ wavenumbers. Significant changes were observed in both the intensity and wavenumber values of these bands on complexation: The bands become relatively more intense, while the wavenumber shifts to the lower values. These changes are strong evidence that complex formation occurs via coordination of the imine nitrogen atom. The medium bands observed right next to the C=N bands (lower wave number) are attributed to the C=C stretching mode of the ring systems.

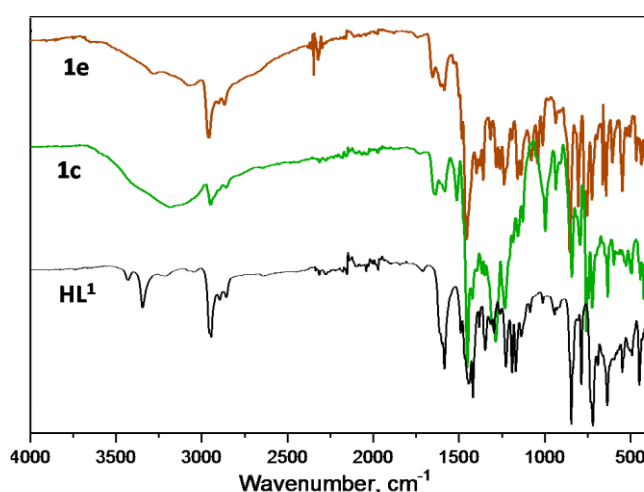


Fig. 6 – The IR spectra of **HL**¹ and its Cu(II) (**1c**) and Pd(II) (**1e**) complexes.

The strong or medium bands at the $1237\text{--}1273\text{ cm}^{-1}$ range can be assigned to phenolic C–O stretching vibrations in the spectra of the ligands and the complexes.²⁷ In the spectra of all the compounds, the characteristic stretching and bending modes of C–H of ring residues are observed between 3074 and 3092 cm^{-1} with medium or weak intensity and at the $779\text{--}813\text{ cm}^{-1}$ region with strong or medium intensity, respectively.^{28,29} The C–Cl stretching vibrations expected to be around 750 cm^{-1} are detected at the range of $755\text{--}776\text{ cm}^{-1}$ as medium bands in all of the compounds.³⁰

In the spectra of **HL**¹ and its complexes, characteristic bands around 2960 cm^{-1} belonging to the stretching vibration $\{\nu(\text{CH})\}$ of the tertiary butyl group are clearly observed.

It is possible to attribute the bands that appear in the IR spectra of the complexes with medium or weak intensity between 612 and 626 cm^{-1} , depending on the ligands, to the $\nu(\text{M}\leftarrow\text{N})$ vibrational mode.³¹ The new medium bands at the

$527\text{--}560\text{ cm}^{-1}$ range in the complexes may be due to the $\nu(\text{M}\leftarrow\text{OC})$ vibration wavenumbers and this finding can be evaluated as information supporting the phenolic oxygen atom coordination.^{5,32,33}

UV-visible spectroscopy

UV-visible spectral data of the compounds obtained in dimethylsulfoxide (DMSO) are presented in Experimental section. UV-visible spectral curves of **HL**² and its complexes are given in Fig. 7.

The electronic spectra of the compounds exhibit intense bands at the $210\text{--}325\text{ nm}$ region: The bands between 210 and 275 nm can be attributed to $\pi \rightarrow \pi^*$ transitions in the rings. The bands in the $275\text{--}325\text{ nm}$ range are due to $\pi \rightarrow \pi^*$ transitions of the azomethine group, while the bands just above 325 nm can be assigned to $n \rightarrow \pi^*$ transitions.³⁴

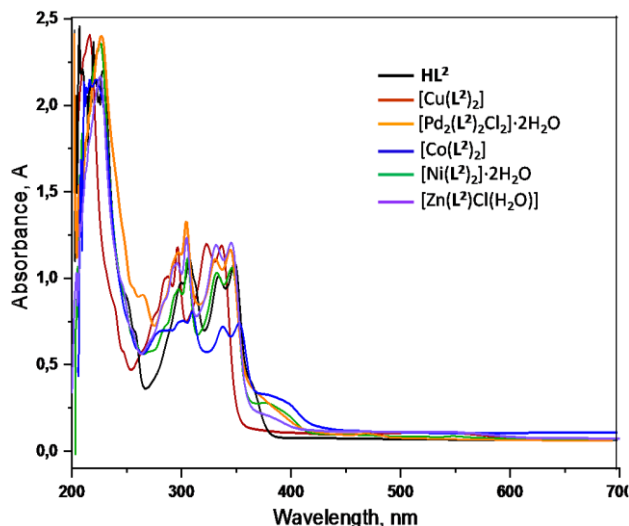


Fig. 7 – The UV-visible spectra of **HL**² and its complexes in DMSO.

The 440–500 nm range bands seen in the ligands are related to intraligand charge transfer transitions. The absorptions at 456 and 465 nm in **1e** and **2e**, respectively, can be assigned to *d-d* transitions and indicate square planar stereochemistry in solution and can be assigned to $^1A_{1g} \rightarrow ^1A_{2g}$ transition.³⁵ The weak bands attributable to *d-d* transitions were detected in the visible region. For instance, the bands observed at 461 and 467 nm in **1a** and **2a**, respectively, indicate a tetrahedral structure and can be attributed to the $^4A_2 \rightarrow ^4T_1(P) (\nu_3)$ transition.³⁶ Similarly, the absorptions at 453 and 459 nm in **1b** and **2b**, respectively, can be attributed to the $^3T_1(F) \rightarrow ^3T_1(P)$ transition in a tetrahedral environment.³⁷ The bands at the 350–550 nm range for **1c** and **2c** can be attributed to LMCT transitions. The fact that no other transitions were observed can be interpreted as **1c** and **2c** having tetrahedral geometry in solution environment.³⁸

Since there are no allowed *d-d* transitions in Zn(II) complexes (**1d** and **2d**), the bands at the 350–450 nm range arise from the intraligand and metal-to-ligand charge transfer transitions.

Fluorescence Spectra

Fluorescence spectral data of the compounds were obtained at a concentration of approximately 1×10^{-4} mol/L in ethanol at room temperature (excitation wavelength: 354 nm). The fluorescence spectral data of the compounds are given in Experimental Section. The fluorescence spectra of **HL**¹ and its complexes are given in Fig. 8.

When the fluorescence spectra of the ligands are examined, it is seen that **HL**¹ and **HL**² emit at 465 and 471 nm, respectively. Accordingly, it is possible to suggest that the *tert*-butyl group causes a slight red shift (shift to higher wavelengths).

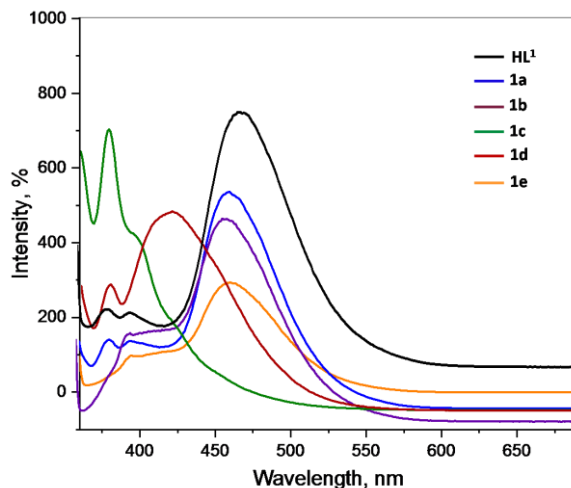


Fig. 8 – Fluorescence spectra of **HL**¹ and its complexes.

The emission wavelength observed in the complexes is as follows: All complexes show a low wavelength shift (blue shift) compared to the ligands. It is observed that both Cu(II) complexes (**1c** and **2c**) significantly reduce or even completely eliminate the fluorescence property (quenching effect). It is observed that the other complexes weaken the fluorescence property.

It was examined fluorescence spectroscopy of 2-(2'-hydroxyphenyl)benzimidazole (HPBz) and found that the most stable form of HPBz is the enol form in the ground state.³⁹⁻⁴¹ However, in the excited singlet state, where the OH group is much more acidic and the C=N nitrogen atom is much more basic compared to the ground state, the stable

structure was reported to be the keto tautomer. This situation is explained by the excited-state intramolecular proton transfer (ESIPT) reaction. Similarly, in our study, it can be argued that the keto form is more stable in the excited state for both **HL**¹ and **HL**² (keto-enol equilibrium for the ligands is given in Fig. 9). A shift towards shorter wavelengths (redshift) is observed in the complexes compared to the ligand, and this can be evaluated as being due to the dominance of the enol form as a result of the formation of the complex.

In the light of the analytical and spectroscopic data obtained, the proposed structures in Fig. 10 can be suggested for the complexes in the study.

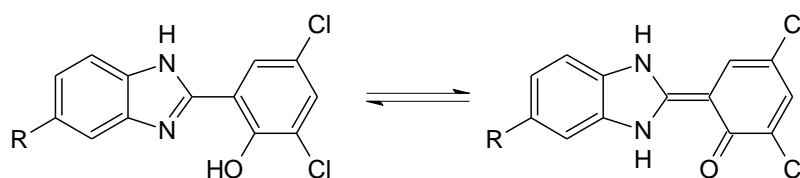
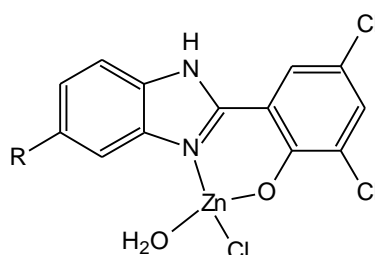
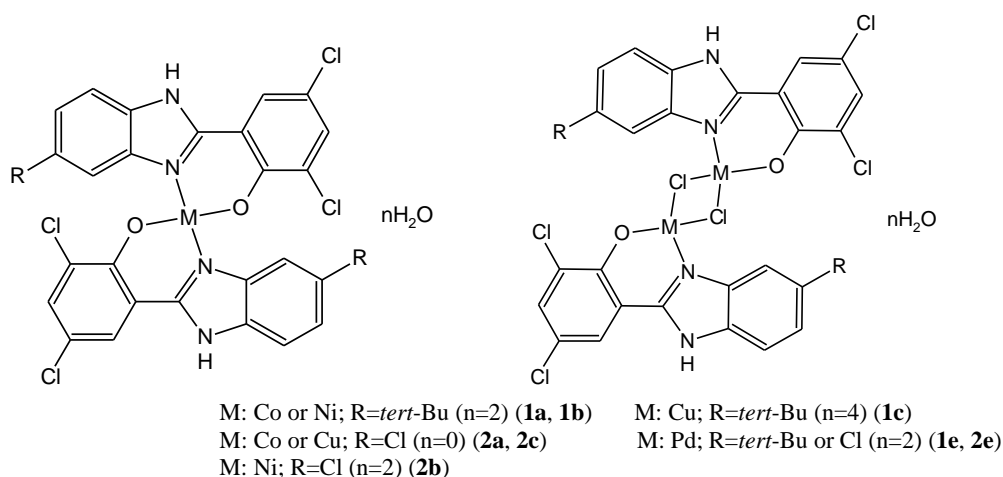


Fig. 9 – Keto-enol tautomer structures of **HL**¹ and **HL**².



1d and **2d** (R=*tert*-Bu or Cl)

Fig. 10 – The proposed coordinations of the complexes.

Antimicrobial activity

In vitro antimicrobial activity values of **HL**¹ and **HL**² and their metal complexes were obtained in terms of MIC, and the results are presented in

Table 1 in comparison with the values of antibiotic and antifungal agents.

When comparing **HL**¹ and **HL**² in the table, it is seen that both benzimidazolylphenol compounds show similar activity, but it is possible to say that

the activity of **HL**² (4-chloro derivative) is relatively better than the other. When the antimicrobial activities of ligands and complexes are compared, it is seen that some complexes exhibit better activity than ligands. For example, the Ni(II) complex of **HL**¹ is seen to be several times more active against *Staphylococcus aureus*, *Staphylococcus epidermidis*, *Escherichia coli*, *Klebsiella pneumoniae* and *Pseudomonas aeruginosa* than the ligand. The Ni(II) complex of **HL**² (**2b**) is seen to have a similar effect, being two times more active against *S. epidermidis* and *E. coli* than the ligand. Considering that the microorganisms in question are bacteria, it can be concluded that they exhibit higher antibacterial activity. It was observed that the Zn(II) and Pd(II) complexes of both ligands (**1d**, **1e**, **2d**, **2e**)

exhibited better activity against all microorganisms tested in the study than the ligand itself. Exhibiting the higher antimicrobial activity of the complexes than the ligands can be explained by the elimination of the phenolic proton and subsequent disappearance of intramolecular hydrogen bonds and the formation of intermolecular hydrogen bonds by the NH proton, the formation of labile complexes, and as a result of these more effective interaction of the complex molecule with the proteins of the microorganisms.

Nevertheless, the MIC values of the compounds used in the study were higher than those of the reference antimicrobials Ciprofloxacin and Amphotericin B. This result shows that the compounds have such weak activity that they cannot compete with the reference substances.

Table 1
In vitro antimicrobial activity of the compounds (MIC, µg/mL)

Compounds	Microorganisms								
	<i>Sa</i> ^{*a}	<i>Se</i> ^a	<i>Ec</i> ^b	<i>Kp</i> ^b	<i>Pa</i> ^b	<i>Pm</i> ^b	<i>Ca</i>	<i>Cp</i>	<i>Ct</i>
HL ¹	312	312	625	625	–	–	625	625	625
1a	–	312	625	–	625	312	312	625	–
1b	39	39	156	78	156	–	156	625	625
1c	156	156	312	625	625	312	–	625	625
1d	625	156	312	625	312	312	312	312	625
1e	39	312	156	156	312	–	156	625	–
HL ²	312	156	625	1250	1250	625	1250	1250	312
2a	–	625	156	625	312	–	312	625	–
2b	–	78	312	625	1250	–	312	312	–
2c	625	625	–	625	625	–	312	312	625
2d	312	78	625	156	312	–	–	625	625
2e	156	156	312	312	312	–	–	625	–
References ^c	0.25	0.25	0.007	0.007	0.125	0.007	0.5	1.0	1.0

* *Sa* *Staphylococcus aureus* ATCC 6538, *Se* *Staphylococcus epidermidis* ATCC 12228, *Ec* *Escherichia coli* ATCC 8739, *Kp* *Klebsiella pneumoniae* ATCC 4352, *Pa* *Pseudomonas aeruginosa* ATCC 1539, *Pm* *Proteus mirabilis* ATCC 14153, *Ca* *Candida albicans* ATCC 10231, *Cp* *Candida parapsilosis* ATCC 22019, *Ct* *Candida tropicalis* ATCC 750

^a, Gram+; ^b, Gram–. –: No antimicrobial effect at 5000 µg/mL and lower dilutions

^c: Ciprofloxacin and Amphotericin B were used for bacteria and fungi, respectively.

Antiviral activity assay

Antiviral activity of the compounds was tested against Parainfluenza Type-2 virus and the results are given at Table 2. It was found that while **HL**¹ inhibited viruses by 32%, **HL**² was effective at a rate of 23%. Considering that **HL**¹ contains *tert*-butyl group and

HL² contains chlorine atom at the same position, it is possible to say that the *tert*-butyl group gives to the molecule a higher virus inhibition feature.

It was observed that the complexes of both ligands showed higher antiviral activity than the ligands except **1b**. It is particularly noteworthy that **2a** showed 50% activity. **1d** and **1e** also have

higher antiviral activity than the ligand (44 and 45%, respectively).

Table 2

Antiviral activity of the compounds	
Compound	Virus inhibition, %
HL¹	32
1a	34
1b	30
1c	37
1d	44
1e	45
HL²	23
2a	50
2b	30
2c	37
2d	28
2e	30
Ribavirin*	100

*Ribavirin: Reference antiviral agent

EXPERIMENTAL

Chemistry and apparatus

All chemicals and solvents were of reagent grade and they were used without further purification.

The devices and techniques used are following: Elemental analysis: LECO combustion analyzer CHNS-932. Melting points: Buchi M-560 melting-point apparatus. Molar conductivity: WTW Cond315i conductivity meter (in DMF at 25 °C). Magnetic measurements: MK1 Sherwood Scientific apparatus (at room temperature by Gouy's method. Diamagnetic corrections were calculated using Pascal's constants). NMR spectroscopy: Varian Unity Inova 500 NMR spectrometer. FT-IR spectroscopy: Bruker Optics Vertex 70 spectrometer with Attenuated Total Reflection (ATR) techniques, between 400 and 4000 cm⁻¹. The Electron Spray Ionization-Mass Spectroscopy (ESI-MS positive ion mode): Thermo Finnigan LCQ Advantage MAX LC/MS/MS (in MeOH). UV-Visible spectra were performed on Shimadzu UV-1800 Spectrophotometer in DMSO. Fluorescence spectra: Shimadzu RF-5301 PC Spectrofluorophotometer ($c = \sim 1 \times 10^{-4}$ mol/L in EtOH). Thermogravimetric studies: TG-60WS Shimadzu, between 30 and 525 °C, with a heating rate of 10 °C/min and air flowing at the rate of 50 mL/min.

Synthesis of the Ligands

A modified method developed by us by utilizing two different methods available in the literature was

applied for synthesis of **HL¹** and **HL²**.⁴²⁻⁴⁴ For **HL¹**, 3,5-dichlorosalicylaldehyde (0.96 g, 5 mmol), 4-*tert*-butylbenzene-1,2-diamine (0.82 g, 5 mmol) and 250 mg H₃BO₃ as catalyst were dissolved in DMF (25 mL) and then this mixture were refluxed for 3 h. After cooling to the room temperature, the reaction mixture was poured into water (250 mL) and then a precipitate was formed. It was filtered, dried and crystallized from ethanol after.

2-(6-*tert*-Butyl-1H-benzimidazol-2-yl)-4,6-dichlorophenol (HL¹): Dirty yellow solid. M.p.: 277 °C. Yield: %71. Found (%): C, 61.14; H, 4.96; N, 8.22. Calcd. (%): C, 60.92; H, 4.80; N, 8.37 for C₁₇H₁₆Cl₂N₂O. MW: 335.22 g/mol. MS (ESI, m/z): 335.3 ([M]⁺, 100%), 337.3 ([M+2H]⁺, 73.3%). FTIR (cm⁻¹): 3354 m,br v(OH), 3227 m v(NH), 3078 m v(CH)_{ar}, 2968 m v(CH)_{al}, 1668 m v(C=N), 1634 m v(C=C), 1572 m, 1495 m, 1452 m, 1393 m, 1273 m v(C-O), 1202 m, 1181 m, 954 m, 857 s, 798 m δ(CH)_{ar}, 732 s v(C-Cl), 648 m, 560 m, 502 m, 460 m. ¹H-NMR (δ_H, ppm): 13.80 s,br (2H, NH+OH), 8.13 d (1H, J=2.5, H3'), 7.67 d (1H, J=2.4, H5'), 7.61 dd,br (2H, J=5.1, 1.3, H5+H7), 7.43 dd (1H, J=8.6, 1.8, H4), 1.37 s (9H, C(CH₃)₃). UV-vis (λ_{max}/nm, in DMSO): 218 m, 248 sh, 296 sh, 306 m, 334 m, 350 m,br. Fluorescence spectroscopy (λ_{max}/nm, in EtOH): 465 m,br.

2,4-Dichloro-6-(6-chloro-1H-benzimidazol-2-yl)phenol (HL²): It was obtained in the same manner as **HL¹**. 4-Chlorobenzene-1,2-diamine (0.713 g, 5 mmol) was used as the reactive diamine compound. Yellowish grey solid. M.p.: 275 °C. Yield: %81. Found (%): C, 50.04; H, 2.42; N, 8.81. Calcd. (%): C, 49.79; H, 2.25; N, 8.93 for C₁₃H₇Cl₃N₂O. MW: 315.30 g/mol. MS (ESI, m/z): 315.3 ([M+2H]⁺, 100%), 313.3 ([M]⁺, 85.5%), 317.3 ([M+4H]⁺, 34.2%). FTIR (cm⁻¹): 3368 m v(OH+NH), 3083 m v(CH)_{ar}, 1633 m v(C=N), 1602 m v(C=C), 1579 m, 1450 m, 1370 m, 1252 m v(C-O), 1184 m, 1060 m, 934 m, 839 m, 798 m δ(CH)_{ar}, 761 m v(C-Cl), 702 m, 593 m, 511 m, 433 m. ¹H-NMR (ppm): 13.78 s,br (2H, NH+OH), 8.12 d (1H, J=2.4, H3'), 7.76 s,br (1H, H7), 7.70 s,br (1H, H5), 7.68 d (1H, J=2.4, H5'), 7.34 dd (1H, J=8.8, 2.0, H4). UV-vis (λ_{max}/nm, in DMSO): 218 m, 227 m, 248 sh, 297 sh, 306 m, 332 m, 348 m, 366 sh. Fluorescence spectroscopy (λ_{max}/nm, in EtOH): 471 m,br.

Synthesis of the Complexes

Appropriate metal salt solutions (1 mmol of Cu(II), Co(II) and Ni(II) chlorides in 10 mL MeOH;

and ZnCl₂ in 10 mL ethyl acetate; K₂PdCl₄ in 10 mL H₂O+MeOH mixture, 6+4, v/v) were added gradually to a solution of the ligand (1 mmol, 335 mg of **HL**¹) in the corresponding solvent {10 mL MeOH for Cu(II), Co(II), Ni(II) and Pd(II) complexes; 10 mL ethylacetate for Zn(II) complex} in the molar ratio 1:1, and heated to reflux for 3 hours. Cu(II) and Pd(II) salts gave immediately precipitates with the ligands in the solvent. The other complex solutions were kept at room temperature, precipitates formed within a few days. The precipitates were filtered, washed with distilled water and kept at room temperature to dry.

[Co(L¹)₂·2H₂O (1a): Brown solid. Yield: 67%. Decomposition point (Dec. p.): >200 °C. Found (%): C, 52.60; H, 4.51; N, 7.11. Calcd. (%): C, 53.49; H, 4.49; N, 7.34 for C₃₄H₃₄Cl₄N₄O₄Co. MW: 763.43 g/mol. Magnetic moment (μ_{eff}): 2.72 BM. Molar conductivity: 33.5 $\Omega^{-1}\text{cm}^2\text{mol}^{-1}$. FT-IR (ATR, cm⁻¹): 3504 m,br $\nu(\text{OH})$, 3215 m $\nu(\text{NH})$, 3080 w,br $\nu(\text{CH})_{\text{ar}}$, 2960 m $\nu(\text{CH})_{\text{al}}$, 2869 m, 1660 m $\nu(\text{C}=\text{N})$, 1622 m $\nu(\text{C}=\text{C})$, 1559 m, 1469 s, 1410 m, 1365 m, 1260 m $\nu(\text{C}-\text{O})$, 1069 s, 952 m, 864 m, 810 m $\delta(\text{CH})_{\text{ar}}$, 762 m $\nu(\text{C}-\text{Cl})$, 739 m, 653 m, 624 m, 560 m, 507 m, 451 m, 416 m. UV-vis ($\lambda_{\text{max}}/\text{nm}$, in DMSO): 217 m, 274 sh, 294 w, 304 m, 331 m, 383 m,br, 461 w. Fluorescence spectra ($\lambda_{\text{max}}/\text{nm}$, in EtOH): 455 m,br. TGA (temp., °C: weight loss, %): 50: 0.7; 75: 3.1 (1.5 mole of H₂O); 100: 4.5 (2 mole of H₂O); 150: 5.5; 200: 5.9; 250: 9.9; 300: 11.5; 350: 39.0; 400: 47.5; 450: 58.1; 500: 75.2. DTA (°C): 232 (exo), 261 (exo), 491 (exo).

[Ni(L¹)₂·2H₂O (1b): Greenish brown solid. Yield: 71%. Dec. p.: >170 °C. Found (%): C, 52.90; H, 4.63; N, 7.18. Calcd. (%): C, 53.51; H, 4.49; N, 7.34 for C₃₄H₃₄Cl₄N₄O₄Ni. MW: 763.16 g/mol. μ_{eff} : 1.21 BM. Molar conductivity: 29.0 $\Omega^{-1}\text{cm}^2\text{mol}^{-1}$. FTIR (cm⁻¹): 3495 m,br $\nu(\text{OH})$, 3245 m $\nu(\text{NH})$, 3077 w,br $\nu(\text{CH})_{\text{ar}}$, 2961 m $\nu(\text{CH})_{\text{al}}$, 2871 m, 1652 m $\nu(\text{C}=\text{N})$, 1628 sh $\nu(\text{C}=\text{C})$, 1564 m, 1495 m, 1361 m, 1271 m $\nu(\text{C}-\text{O})$, 1165 m, 1077 s, 965 m, 910 m, 859 m, 800 m $\delta(\text{CH})_{\text{ar}}$, 760 m $\nu(\text{C}-\text{Cl})$, 712 m, 653 m, 625 m, 564 m, 497 m, 454 m, 413 m. UV-vis ($\lambda_{\text{max}}/\text{nm}$, in DMSO): 222 m, 247 sh, 295 sh, 307 m, 331 m, 347 m, 384 m,br, 453 w. Fluorescence spectra ($\lambda_{\text{max}}/\text{nm}$, in EtOH): 453 m,br. TGA (temp., °C: weight loss, %): 50: 0.5; 75: 4.2 (~2 mole of H₂O); 100: 5.1; 150: 7.4; 200: 13.5; 250: 16.6; 300: 20.1; 350: 25.0; 400: 27.1; 450: 37.2; 500: 47.0. DTA (°C): 68 (exo), 161 (exo), 320 (exo), 447 (exo).

[Cu₂(L¹)₂Cl₂·4H₂O (1c): Greenish brown solid. Yield: 76%. Dec. p.: >200 °C. Found (%): C,

43.61; H, 4.02; N, 6.15. Calcd. C, 43.51; H, 4.08; N, 5.97 (%) for C₃₄H₃₄Cl₆N₄O₆Cu₂. MW: 938.50 g/mol. μ_{eff} : 1.25 BM per Cu(II) ion. Molar conductivity: 28.7 $\Omega^{-1}\text{cm}^2\text{mol}^{-1}$. FTIR (cm⁻¹): 3187 m,br $\nu(\text{OH})$, 3124 w,br $\nu(\text{NH})$, 2956 m $\nu(\text{CH})_{\text{al}}$, 2865 m, 1651 m $\nu(\text{C}=\text{N})$, 1597 m $\nu(\text{C}=\text{C})$, 1525 m, 1463 s, 1300 m, 1243 m $\nu(\text{C}-\text{O})$, 1172 m, 1011 m, 949 m, 861 m, 810 m $\delta(\text{CH})_{\text{ar}}$, 755 m $\nu(\text{C}-\text{Cl})$, 649 m, 612, 542 m, 513 m, 440 m, 410 m. UV-vis ($\lambda_{\text{max}}/\text{nm}$, in DMSO): 205 m, 224 m, 257 sh, 294 m, 306 m, 351 sh, 363 m,br, 381 sh. Fluorescence spectra ($\lambda_{\text{max}}/\text{nm}$, in EtOH): 379 m, 398 sh. TGA (temp., °C: weight loss, %): 50: 2.8 (~1 mole of H₂O); 75: 5.8; 100: 7.5 (4 moles of H₂O); 150: 9.5; 200: 11.2; 250: 14.6; 300: 17.6; 350: 21.0; 400: 26.3; 450: 56.6; 500: 64.1. DTA (°C): 47 (exo), 136 (exo), 231 (exo), 407 (exo).

[Zn(L¹)Cl(H₂O)] (1d): Dark yellow solid. Yield: 67%. Dec. p.: >200 °C. Found (%): C, 45.30; H, 6.04; N, 6.10. Calcd. (%): C, 45.06; H, 3.78; N, 6.18 for C₁₇H₁₇Cl₃N₂O₂Zn. MW: 453.10 g/mol. Molar conductivity: 29.1 $\Omega^{-1}\text{cm}^2\text{mol}^{-1}$. FTIR (cm⁻¹): 3412 m,br $\nu(\text{OH})$, 3163 m,br $\nu(\text{NH})$, 3092 w,br $\nu(\text{CH})_{\text{ar}}$, 2961 m $\nu(\text{CH})_{\text{al}}$, 2869 m, 1658 m $\nu(\text{C}=\text{N})$, 1598 m $\nu(\text{C}=\text{C})$, 1575 m, 1463 s, 1412 m, 1367 m, 1249 m $\nu(\text{C}-\text{O})$, 1233 m, 1158 m, 1101 m, 979 m, 918 m, 865 m, 809 m $\delta(\text{CH})_{\text{ar}}$, 763 m $\nu(\text{C}-\text{Cl})$, 731 m, 645 m, 604 m, 540 m, 493 m, 425 m. ¹H-NMR (ppm): 13.46 s,br (1H, NH), 8.02 d (1H, J=2.4, H3'), 7.54 d,br (1H, J=2.9, H5'), 7.48 d (1H, J=8.8, H4), 7.46 d (1H, J=2.9, H7), 7.34 d,br (1H, J=7.8, H5), 1.33 s (9H, C(CH₃)₃). UV-vis ($\lambda_{\text{max}}/\text{nm}$, in DMSO): 225 m, 256 m,br, 295 m, 307 m,br, 353 sh, 375 m,br. Fluorescence spectra ($\lambda_{\text{max}}/\text{nm}$, in EtOH): 378 m, 421 m,br. TGA (temp., °C: weight loss, %): 50: 0.7; 75: 1.3; 100: 1.9; 150: 2.5; 200: 3.6 (~1 moles of H₂O); 250: 8.3; 300: 16.1; 350: 22.6; 400: 31.0; 450: 64.7; 500: 71.0. DTA (°C): 153 (endo), 247 (exo), 292 (exo), 421 (exo).

[Pd₂(L¹)₂Cl₂·2H₂O (1e): Light brown solid. Yield: 72%. Dec. p.: >200 °C. Found (%): C, 41.10; H, 3.64; N, 5.78. Calcd. (%): C, 41.32; H, 3.47; N, 5.67 for C₁₇H₁₇Cl₃N₂O₂Pd. MW: 494.11 g/mol. Molar conductivity: 47.5 $\Omega^{-1}\text{cm}^2\text{mol}^{-1}$. FTIR (cm⁻¹): 3280 m,br $\nu(\text{OH})$, 3150 m,br $\nu(\text{NH})$, 3074 m,br $\nu(\text{CH})_{\text{ar}}$, 2960 m $\nu(\text{CH})_{\text{al}}$, 2866 m, 1658 m $\nu(\text{C}=\text{N})$, 1613 m $\nu(\text{C}=\text{C})$, 1591 m, 1461 m, 1402 m, 1367 m, 1245 m $\nu(\text{C}-\text{O})$, 1164 m, 1087 m, 944 m, 860 s, 813 m $\delta(\text{CH})_{\text{ar}}$, 776 m $\nu(\text{C}-\text{Cl})$, 735 m, 650 m, 617 m, 554 m, 477 m, 445 m, 423 m. ¹H-NMR (ppm): 13.72 s,br (1H, NH), 8.23 d (1H,

J=2.2, H3'), 7.67 d (1H, J=2.5, H5'), 7.62 d (1H, J=8.5, H4), 7.59 d (1H, J=2.7, H7), 7.42 dd (1H, J=8.6, 1.7, H5), 1.37 s (9H, C(CH₃)₃). UV-Vis (λ_{max} /nm, in DMSO): 220 m, 247 sh, 292 m, br, 304 m, 331 m, 347 m, 456 w. Fluorescence spectra (λ_{max} /nm, in EtOH): 394 w, 457 m, br. TGA (temp., °C: weight loss, %): 50: 2.0; 75: 3.0 (~1 mole of H₂O); 100: 3.4; 150: 4.7; 200: 7.8; 250: 9.2; 300: 12.1; 350: 21.3; 400: 27.6; 450: 47.2; 500: 59.1. DTA (°C): 225 (endo), 291(endo), 420 (exo).

[Co(L²)₂] (2a): Brown solid. Yield: 70%. Dec. p.: >250 °C. Found (%): C, 46.02; H, 1.93; N, 8.12. Calcd. (%): C, 45.65; H, 1.77; N, 8.19 for C₂₆H₁₂Cl₆N₄O₂Co. MW: 684.05 g/mol. μ_{eff} : 2.81 BM. Molar conductivity: 25.0 $\Omega^{-1}\text{cm}^2\text{mol}^{-1}$. FTIR (cm⁻¹): 3370 m, br v(OH), 3273 w v(NH), 3083 w, br v(CH)_{ar.}, 1624 m v(C=N), 1589 m v(C=C), 1533 m, 1455 s, 1372 m, 1254 m v(C-O), 1061 m, 935 m, 859 m, 798 m δ (CH)_{ar.}, 763 m v(C-Cl), 704 m, 624 m, 595 m, 511 m, 474 m, 430 m. UV-Vis (λ_{max} /nm, in DMSO): 236 m, 255 sh, 296 sh, 305 m, 330 m, br, 343 m, 386 w, br, 467 w. Fluorescence spectra (λ_{max} /nm, in EtOH): 423 sh, 462 m, br. TGA (temp., °C: weight loss, %): 50: 0.3; 75: 0.4; 100: 0.5; 150: 0.9; 200: 2.4; 250: 3.6; 300: 32.1; 350: 41.9; 400: 57.6; 450: 68.6; 500: 72.6. DTA (°C): 215 (exo), 292 (exo), 435 (exo).

[Ni(L²)₂·2H₂O] (2b): Greenish brown solid. Yield: 68%. Dec. p.: >200 °C. Found (%): C, 43.19; H, 2.38; N, 7.61. Calcd. (%): C, 43.38; H, 2.24; N, 7.78 for C₂₆H₁₆Cl₆N₄O₄Ni. MW: 719.84 g/mol. μ_{eff} : 1.31 BM. Molar conductivity: 37.5 $\Omega^{-1}\text{cm}^2\text{mol}^{-1}$. FTIR (cm⁻¹): 3511 m, br v(OH), 3271 m v(NH), 3084 m v(CH)_{ar.}, 1626 m v(C=N), 1610 m v(C=C), 1586 m, 1455 s, 1373 m, 1306 m, 1255 m v(C-O), 1188 m, 1087 m, 1061 m, 935 m, 860 m, 839 m, 799 m δ (CH)_{ar.}, 764 m v(C-Cl), 706 m, 596 m, 511 m, 431 m. UV-vis (λ_{max} /nm, in DMSO): 223 m, 282 sh, 297 w, 305 m, 332 m, 346 m, 389 w, br, 459 w. Fluorescence spectra (λ_{max} /nm, in EtOH): 424 sh, 463 m, br. TGA (temp., °C: weight loss, %): 50: 4.3; 75: 5.1 (2 mole of H₂O); 100: 5.5; 150: 7.7; 200: 10.4; 250: 21.6; 300: 37.1; 350: 51.9; 400: 55.6; 450: 58.6; 500: 65.7. DTA (°C): 48 (exo), 192 (exo), 365 (exo).

[Cu(L²)₂] (2c): Brown solid. Yield: 74%. Dec. p.: >230 °C. Found (%): C, 45.15; H, 1.88; N, 8.04. Calcd. (%): C, 45.35; H, 1.76; N, 8.14 for C₂₆H₁₂Cl₆N₄O₂Cu. MW: 686.66 g/mol. μ_{eff} : 1.62 BM. Molar conductivity: 24.1 $\Omega^{-1}\text{cm}^2\text{mol}^{-1}$. FTIR (cm⁻¹): 3609 m, 3325 m, br v(NH), 3125 w v(OH),

3083 m, br v(CH)_{ar.}, 2978 m v(CH)_{al.}, 1619 m v(C=N), 1592 m v(C=C), 1523 m, 1458 s, 1241 m v(C-O), 1144 m, 1048 m, 1007 m, 935 m, 868 m, 812 m, 779 m δ (CH)_{ar.}, 761 m v(C-Cl), 734 m, 648 m, 597 m, 530 m, 458 m, 433 m. UV-vis (λ_{max} /nm, in DMSO): 224 m, 246 sh, 283 sh, 295 m, 304 m, 331 m, 346 m, 532 w, br. Fluorescence spectra (λ_{max} /nm, in EtOH): 394 m, br, 423 sh. TGA (temp., °C: weight loss, %): 50: 0.1; 75: 0.2; 100: 0.3; 150: 1.4; 200: 2.4; 250: 20.7; 300: 38.3; 350: 52.8; 400: 60.1; 450: 64.7; 500: 70.1. DTA (°C): 195 (exo), 221 (exo), 375 (exo).

[Zn(L²)Cl(H₂O)] (2d): Light brown solid. Yield: 68%. Dec. p.: >200 °C. Found (%): C, 36.01; H, 2.02; N, 6.36. Calcd. (%): C, 36.19; H, 1.87; N, 6.49 for C₁₃H₈Cl₄N₂O₂Zn. MW: 431.44 g/mol. Molar conductivity: 33.5 $\Omega^{-1}\text{cm}^2\text{mol}^{-1}$. FTIR (cm⁻¹): 3335 m, br v(OH), 3207 m, br v(NH), 3088 w, br v(CH)_{ar.}, 1629 m v(C=N), 1600 m v(C=C), 1554 m, 1495 m, 1457 s, 1298 m, 1260 m v(C-O), 1144 m, 1058 m, 1017 m, 937 m, 869 m, 806 m δ (CH)_{ar.}, 771 m v(C-Cl), 635 m, 596 m, 512 m, 450 m, 426 m. ¹H-NMR (ppm): 13.70 s, br (1H, NH), 8.14 d (1H, J=2.5, H3'), 7.78 d (1H, J=8.6, H4), 7.70 s, br (1H, J=2.5, H7), 7.41 d (1H, J=2.3, H5'), 7.35 dd (1H, J=8.6, 2.0, H5). UV-vis (λ_{max} /nm, in DMSO): 226 m, 248 sh, 295 m, 305 m, 332 m, 346 m, 387 w, 537 w. Fluorescence spectra (λ_{max} /nm, in EtOH): 376 m, 422 w, 461 m, br. TGA (temp., °C: weight loss, %): 50: 0.6; 75: 1.2; 100: 1.8; 150: 2.6; 200: 3.7 (~1 moles of H₂O); 250: 8.5; 300: 17.2; 350: 24.5; 400: 34.2; 450: 66.2; 500: 74.2. DTA (°C): 157 (endo), 251 (exo), 430 (exo).

[Pd₂(L²)₂Cl₂·2H₂O] (2e): Light brown solid. Yield: 73%. Dec. p.: >170 °C. Found (%): C, 32.85; H, 1.66; N, 5.85. Calcd. (%): C, 33.05; H, 1.71; N, 5.93 for C₁₃H₈Cl₄N₂O₂Pd. MW: 472.45 g/mol. Molar conductivity: 29.3 $\Omega^{-1}\text{cm}^2\text{mol}^{-1}$. FTIR (cm⁻¹): 3402 m, br v(OH+NH), 3107 m v(CH)_{ar.}, 1615 m v(C=N), 1594 m v(C=C), 1552 m, 1509 m, 1457 s, 1297 m, 1244 m v(C-O), 1163 m, 1060 m, 1015 m, 932 m, 853 m, 804 m δ (CH)_{ar.}, 776 m v(C-Cl), 731 m, 665 m, 626 m, 597 m, 552 m, 518 m, 460 m, 417 m. ¹H-NMR (ppm): 13.82 s, br (1H, NH), 8.19 d (1H, J=2.5, H3'), 7.74 d (1H, J=8.1, H4), 7.69 d (1H, J=2.5, H7), 7.51 d (1H, J=2.0, H5'), 7.35 dd (1H, J=8.6, 1.9, H5). UV-vis (λ_{max} /nm, in DMSO): 225 m, 264 w, 294 sh, 304 m, 331 m, 345 m, br, 389 m, br, 465 w. Fluorescence spectra (λ_{max} /nm, in EtOH): 458 m. TGA (temp., °C: weight loss, %): 50: 1.8; 75: 3.1 (~1 mole of

H₂O); 100: 3.5; 150: 4.8; 200: 8.0; 250: 10.6; 300: 14.2; 350: 24.5; 400: 30.4; 450: 48.6; 500: 61.4. DTA (°C): 230 (endo), 301 (exo), 416 (exo).

Determination of antibacterial and antifungal activity

Antimicrobial activities of the ligands and complexes were investigated against standard ATCC strains of bacteria and fungi by the microbroth dilutions way according to the Clinical and Laboratory Standards Institute (CLSI) guidance.⁴⁵⁻⁴⁶ The antimicrobial activity procedure and the microorganisms used are the same as in our previous study.¹⁶ The experiments were carried out in duplicate.

Antiviral activity assay

For Parainfluenza Type-2 virus (PIV-2), African green monkey kidney cell line (VERO, ATCC) was cultured in Dulbecco's modified Eagle's medium (Wisent, MULTICELL) supplemented with 10% fetal bovine serum (FBS; Sigma), 100 U/mL penicillin, and 100 µg/mL streptomycin. The PIV-2 and cells were maintained at 37°C under 5% CO₂ atmosphere.

An experiment was conducted based on the plaque formation test for PIV-2 strain that grown on VERO cell culture.⁴⁷ VERO cells were infected with PIV-2 at 100 PFU per well, one of the wells was used as a control and the antiviral activities of the samples were tested in the other wells. The virus-infected control (Ribavirin) well was accepted as 100%, and the efficacy results were calculated as a percentage by comparing this control value. The concentration of the compounds is 10 mg/mL.

CONCLUSION

Benzimidazolylphenols are interesting compounds due to their properties such as strong chelators and having a wide range of activities. In this study, two derivatives of 2-(1*H*-benzimidazol-2-yl)-4,6-dichlorophenol, which have tertiary butyl and chlorine substituents in the benzimidazole part, and their Co(II), Ni(II), Cu(II), Zn(II) and Pd(II) complexes were obtained. Physicochemical (elemental analysis, UV-vis, FT-IR, fluorescence, ¹H-NMR spectroscopic techniques as well as magnetic moment and molar conductivity

measurements) properties and antibacterial, antifungal and antiviral effects of the compounds were investigated and compared.

According to molar conductivity measurements, all of the complexes showed non-ionic character in DMF. It was observed that Co(II) and Ni(II) ions preferred to form complexes with both ligands at a 1:2 M:L ratio, while this ratio is 1:1 in Zn(II) and Pd(II) complexes. The antibacterial and antifungal activities of the compounds were tested against certain bacteria and fungi and observed that the chloro derivative (**HL**²) showed slightly higher activity than the *tert*-butyl derivative (**HL**¹). It is noteworthy that the Ni(II), Zn(II) and Pd(II) complexes of both ligands show higher activity against bacteria than the ligands. The antiviral activity of the compounds was tested against Parainfluenza Type-2 virus and all the compounds were found to show mediocre activity. Among the antiviral activity values, **HL**¹ showed higher activity than **HL**², which can be evaluated as the antiviral effect enhancing effect of the *tert*-butyl group. On the other hand, another interesting result is that the antiviral activities of the complexes were found to be higher than the ligands.

Acknowledgment. This work was supported by Scientific Research Projects Coordination Unit of Istanbul University-Cerrahpasa (Project number: 36370) and The Scientific and Technological Research Council of Türkiye (TUBITAK, Project number: 123Z795).

REFERENCES

1. Y. Ma, H. Liu, C. Li, Y. Zhang, M. Lv, D. Mu, S. Yin and R. Liu, *J. Mol. Struct.*, **2024**, 1309, Article ID 138172.
2. W.-Y. Zhu, K. Liu and X. Zhang, *Sens. Diagn.*, **2023**, 2, 665–675.
3. R. Sathyanarayana, V. Kumar, G. H. Pujar, B. Poojary, M. K. Shankar and S. Yallappa, *J. Photochem. Photobiol. A: Chem.*, **2020**, 401, Article ID 112751.
4. A. Tavman, M. Hacıoğlu, D. Gürbüz, A. Çınarlı, M. A. F. Öksüzömer and A. S. Birteksöz Tan, *Bull. Chem. Soc. Ethiop.*, **2019**, 33, 451–466.
5. A. Tavman, N. M. Agh-Atabay, S. Güner, F. Gücin and B. Dülger, *Transit. Met. Chem.*, **2007**, 32, 172–179.
6. A. Tavman, S. İkiz, A. F. Bağcıgil, Y. N. Özgür and S. Ak, *Bull. Chem. Soc. Ethiop.*, **2010**, 24, 391–400.
7. A. Tavman, S. İkiz, A. F. Bağcıgil, Y. N. Özgür and S. Ak, *J. Serb. Chem. Soc.*, **2009**, 74, 537–548.
8. A. Tavman, S. İkiz, A. F. Bağcıgil, Y. N. Özgür and S. Ak, *Russ. J. Inorg. Chem.*, **2010**, 55, 215–222.
9. A. Tavman, A. Çınarlı, D. Gürbüz and A. S. Birteksöz, *J. Iran. Chem. Soc.*, **2012**, 9, 815–825.
10. A. Tavman and A. S. Birteksöz, *Rev. Inorg. Chem.*, **2009**, 29, 255–272.
11. A. Tavman, A. S. Birteksöz and F. Öksüzömer, *S. Afr. J. Chem.*, **2012**, 65, 150–158.

12. A. Tavman, D. Gürbüz, A. A. Karaçelik, D. N. Çolak, D. Efe and A. Çınarlı, *Rev. Roum. Chim.*, **2024**, *69*(3-4), 201–214.
13. A. Tavman, I. Boz and A. S. Birteksöz, *Spectrochim. Acta*, **2010**, *A77*, 199–206.
14. A. Tavman, I. Boz, A. S. Birteksöz and A. Çınarlı, *J. Coord. Chem.*, **2010**, *63*, 1398–1410.
15. A. Tavman, D. Gürbüz, Ş. Öksüz and A. Çınarlı, *Mor. J. Chem.*, **2018**, *6*(2), 328–341.
16. A. Tavman, A. Z. Elmal, D. Gürbüz, M. Hacıoğlu, A. S. Birteksöz Tan and A. Çınarlı, *Rev. Roum. Chim.*, **2023**, *68*, 49–59.
17. A. Hernández-Morales, J.M. Rivera, A. López-Monteón, S. Lagunes-Castro, S. Castillo-Blum, K. Cureño-Hernández, A. Flores-Parra, O. Villaseñor-Granados and R. Colorado-Peralta, *J. Inorg. Biochem.*, **2019**, *201*, Article ID 110842.
18. K. Mahmood, Z. Akhter, M. A. Asghar, B. Mirza, H. Ismail, F. Liaqat, S. Kalsoom, A. R. Ashraf, M. Shabbir, M. A. Qayyum and V. McKee, *J. Biomol. Struct. Dyn.*, **2020**, *38*(6), 1670–1682.
19. X. Totta, A. A. Papadopoulou, A. G. Hatzidimitriou, A. Papadopoulos and G. Psomas, *J. Inorg. Biochem.*, **2015**, *145*, 79–93.
20. A. Kerflani, K. S. Larbi, A. Rabahi, A. Bouchoucha, S. Zaater and S. Terrachet-Bouaziz, *Inorg. Chim. Acta*, **2022**, *529*, Article ID 120659.
21. W. J. Geary, *Coord. Chem. Rev.* **1971**, *7*, 81–122.
22. E. Alterhoni, A. Tavman, M. Hacıoğlu, O. Şahin and A. S. Birteksöz Tan, *J. Mol. Struct.*, **2021**, *1229*, Article ID 129498.
23. D. M. Jenkins, A. J. Di Bilio, M. J. Allen, T. A. Betley and J. C. Peters, *J. Am. Chem. Soc.*, **2002**, *124*, 15336–15350.
24. R. T. Stibrany, S. Fox, P. K. Bharadwaj, H. J. Schugar and J. A. Potenza, *Inorg. Chem.*, **2005**, *44*, 8234–8242.
25. B. Jeragh, and A. A. El-Asmy, *Spectrochim. Acta*, **2014**, *A130*, 546–552.
26. R. M. El-Shazly, G. A. A. Al-Hazmi, S. E. Ghazy, M. S. El-Shahawi and A. A. El-Asmy, *Spectrochim. Acta*, **2005**, *A61*, 243–252.
27. R. Singh, A. Prakash, S. K. Dhiman, B. Balagurumurthy, A. K. Arora, S. K. Puri and T. Bhaskar, *Bioresour. Technol.*, **2014**, *165*, 319–322; X.-H. Guan, C. Shang and G.-H. Chen, *Chemosphere*, **2006**, *6*, 2074–2081; E. Kaki, A. Altnidal, B. Salih and Ö. Bekaroglu, *Dalton Trans.*, **2015**, *44*, 8293–8299.
28. A. Tavman, N.M. Agh-Atabay, A. Neshat, F. Gücin, B. Dülger and D. Hacıu, *Transit. Metal Chem.*, **2006**, *31*, 194–200.
29. K. Nakamoto, *Infrared and Raman Spectra of Inorganic and Coordination Compounds*, Part B, 5th edn., John Wiley & Sons, Inc., New York, 1997.
30. N. Sundaraganesan, C. Meganathan, B. Anand and C. Lapouge, *Spectrochim. Acta A*, **2007**, *66*, 773–780.
32. A. Tavman, N. M. Agh-Atabay, A. Neshat, F. Gücin, B. Dülger and D. Hacıu, *Transit. Metal Chem.*, **2006**, *31*, 194–200.
31. V. T. Yılmaz, S. Hamamci, Ö. Andac and K. Güven, *Z. Anorg. Allg. Chem.*, **2003**, *629*, 172–176.
33. V. M. Leovac, L. S. Jovanovic, V. S. Cesljevic, L. J. Bjelica, V. B. Arion and N. V. Gerbeleu, *Polyhedron*, **1994**, *13*, 3005–3014.
34. Y. Kaya, H. Mutlu and G. Irez, *Gazi Univ. J. Sci.*, **2010**, *23*, 13–18.
35. D. Pardaeva, A. Tavman, D. Gürbüz, M. Hacıoğlu, F. N. Yılmaz, O. Şahin, A. S. Birteksöz Tan and A. Çınarlı, *Rev. Roum. Chim.*, **2024**, *69*, 83–96.
36. R. A. Ahmadi and S. Amani, *Molecules*, **2012**, *17*, 6434–6448; A. B. P. Lever, “Inorganic Electronic Spectroscopy”, second edition, Elsevier: Amsterdam, The Netherlands, 1982.
37. N. El-wakiel, M. El-keiy and M. Gaber, *Spectrochim. Acta*, **2015**, *A147*, 117–123.
38. I. Shimizu, Y. Morimoto, G. Velmurugan, T. Gupta, S. Paria, T. Ohta, H. Sugimoto, T. Ogura, P. Comba and S. Itoh, *Chem.-Eur. J.*, **2019**, *25*, 11157–11165.
39. X.-F. Yang, H. Qi, L. Wang, Z. Su and G. Wang, *Talanta*, **2009**, *80*, 92–97.
40. M. Mosquera, M. C. R. Rodriguez and F. Rodriguez-Prieto, *J. Phys. Chem. A*, **1997**, *101*, 2766–2772.
41. F. Rodriguez-Prieto, J. C. Penedo and M. Mosquera, *J. Chem. Soc. Faraday Trans.*, **1998**, *94*, 2775–2782.
42. H. F. Ridley, G. W. Spickett and G. M. Timmis, *J. Het. Chem.*, **1965**, *2*, 453–456.
43. Z. Karimi-Jaberi and M. Amir, *J. Chem.*, **2012**, *9*, 167–171.
44. O. S. Ürgüt, A. Tavman and M. Gürkan Eser, *Chem. J. Mold.*, **2022**, *17*, 73–83.
45. Clinical and Laboratory Standards Institute (CLSI). Performance Standards for Antimicrobial. Document M100-Ed.31., Wayne, PA, USA, 2021.
46. Clinical and Laboratory Standards Institute (CLSI). Reference Method for Broth Dilution Antifungal Susceptibility Testing of Yeasts: Approved Standard-Third Edition. M27-A3, Wayne, PA, USA, 2012.
47. K. Fukushima, T. Takahashi, M. Takaguchi, H. Ueyama, S. Ito, Y. Kurebayashi, T. Kawanishi, J. L. McKimm-Breschkin, T. Takimoto, A. Minami and T. Suzuki. *Biol. Pharm. Bull.*, **2011**, *34*, 996–1000.

